

Radial Color Gradient and Main Sequence Mass Segregation in M30 (NGC 7099)¹

Justin H. Howell and Puragra Guhathakurta²

UCO/Lick Observatory, Department of Astronomy & Astrophysics,
University of California, Santa Cruz, California 95064, USA
Email: jhhowell@ucolick.org, raja@ucolick.org

and

Amy Tan

University of California, Davis, California 95616, USA
Email: aatan@ucdavis.edu

ABSTRACT

It has long been known that the post-core-collapse globular cluster M30 (NGC 7099) has a bluer-inward color gradient, and recent work suggests that the central deficiency of bright red giant stars does not fully account for this gradient. This study uses *Hubble Space Telescope* Wide Field Planetary Camera 2 images in the F439W and F555W bands, along with ground-based CCD images with a wider field of view for normalization of the non-cluster background contribution, and finds $\Delta(B - V) \sim +0.3$ mag for the overall cluster starlight over the range $2''$ to $\gtrsim 1'$ in radius. The slope of the color profile in this radial range is: $\Delta(B - V)/\Delta \log(r) = 0.20 \pm 0.07$ mag dex⁻¹, where the quoted uncertainty accounts for Poisson fluctuations in the small number of bright evolved stars that dominate the cluster light. We explore various algorithms for artificially redistributing the light of bright red giants and horizontal branch stars uniformly across the cluster. The traditional method of redistribution in proportion to the cluster brightness profile is shown to be inaccurate. There is no significant residual color gradient in M30 after proper uniform redistribution of all bright evolved stars; thus the color gradient in M30's central region appears to be due entirely to post-main-sequence stars. Two classes of plausible

¹Based on observations with the NASA/ESA *Hubble Space Telescope*, obtained at the Space Telescope Science Institute, which is operated by the Association of Universities for Research in Astronomy, Inc., under NASA contract NAS 5-26555.

²Alfred P. Sloan Research Fellow

dynamical models, Fokker-Planck and multimass King models, are combined with theoretical stellar isochrones from Bergbusch & Vandenberg (1992) and from D’Antona and collaborators to quantify the effect of mass segregation of main sequence stars. In all cases, mass segregation of main sequence stars results in $\Delta(B - V) \sim -0.06$ to $+0.02$ mag over the range $r = 20'' - 80''$; this is consistent with M30’s residual color gradient within measurement error. The observed fraction of evolved star light in the B and V bands agrees with the corresponding model predictions at small radii but drops below it for $r \gtrsim 20''$.

Subject headings: globular clusters: individual (M30, NGC 7099) — globular clusters: general

1. Introduction

Due to their high density, cores of globular clusters serve as excellent laboratories for studying stellar interactions and the resulting changes in stellar populations (Hut et al. 1992; Meylan & Heggie 1997). In particular, a small fraction of clusters known as post core collapse (PCC) clusters are characterized by extremely high central densities and tend to have color gradients in the sense of becoming bluer inward. Though several authors have shown that central depletion of bright red giant branch (RGB) stars is an important contributor to the color gradient in these clusters (cf. Piotto, King, & Djorgovski 1988; Burgarella & Buat 1996; Guhathakurta et al. 1998, hereafter GWYSB), a satisfactory explanation of the underlying physical cause of this RGB depletion has proven elusive (Djorgovski et al. 1991). Most globular clusters are well fit by King models (KMs; King 1962) and very few of these show any such color gradient. Even the KM clusters that are suspected to have a color gradient (e.g., NGC 4147) are all quite centrally concentrated so that the distinction between KM and PCC clusters is unclear in these cases (Djorgovski & Piotto 1992, 1993).

M30 is a prototypical PCC cluster, with one of the best-studied color gradients of all globular clusters (Williams & Bahcall 1979; Chun & Freeman 1979; Cordoni & Aurière 1984; Peterson 1986; Piotto et al. 1988; Burgarella & Buat 1996; GWYSB). This gradient has traditionally been explained by a deficiency of red giants and asymptotic giant branch stars near the cluster center, but Burgarella & Buat (1996) found that this central deficiency does not account for the observed color gradient, and GWYSB have independently suggested that the central evolved star deficit only produces one third of the observed color gradient in M30, and all evolved stellar populations put together produce less than half of the observed

gradient. A possible explanation for the rest of the color gradient is mass segregation of main sequence stars, since stars near the main sequence turnoff, with higher mass and bluer color, are expected to be more centrally concentrated than the fainter, redder, and less massive stars.

This paper reexamines the radial color profile of M30’s starlight using *Hubble Space Telescope* (*HST*) Wide Field Planetary Camera 2 (WFPC2) images and wider field ground-based images, tests methods for redistributing the light of bright stars, and addresses the question of whether main sequence mass segregation produces the necessary color gradient to explain the observations. Observations of M30’s color gradient and methods for uniformly redistributing the light of bright evolved stars are described in §2. Calculations of the effects of main sequence mass segregation are presented in §3, and §4 contains a summary of the main points of the paper.

2. Observed Color Gradient

2.1. Non-Cluster “Background” Brightness

In order to study the color of the cluster starlight, it is necessary to determine and correct for the “background” level in the *HST*/WFPC2 images. The term “background” includes all non-cluster contributions to the total light, including foreground zodiacal light, extragalactic background light, and even non-astrophysical artifacts such as low level residual cosmic rays and hot pixels. GWYSB estimated this background to be 0.094 ADU pixel⁻¹ in F439W and 0.054 ADU pixel⁻¹ in F555W based on visually selected regions of the image more than 1’5 from the cluster center and away from resolved stars. This technique could be biased in either direction: the background would be overestimated if unresolved cluster starlight contributes significantly to the background over the entire image, or underestimated if atypically dark regions were selected that systematically avoid, for example, hot pixels, residual cosmic rays, and/or background galaxies.

This paper uses a combination of *HST*/WFPC2 data and short ground-based *B*- and *V*-band CCD exposures of M30 provided by Mike Bolte (see Bolte 1987; Sandquist et al. 1999 for details) to determine the background brightness in the WFPC2 images, in contrast to the method used by GWYSB. The ground-based images are used only for background estimation and not for stellar photometry. They cover a sufficiently large field of view that unresolved cluster light is unlikely to affect measurements of the background in the far corners of the CCD frames. The background in these images includes a dominant atmospheric airglow component in addition to the sources listed above. The mean *B*- and

V -band background brightnesses are measured in selected regions of these images located at projected distances of $r \sim 3' - 4.7'$ and $r \sim 8' - 11'$, respectively, from the cluster center; these background estimates are then subtracted from the images. Note, the ground-based B data consist of two images, a core pointing covering most of the WFPC2 field of view, and a southwest pointing which overlaps the core pointing but not the WFPC2 field. Since the core image extends only to $r \sim 3'$, the southwest image is used for background estimation. This background estimate is bootstrapped to the core image using a difference image: core image minus registered, background-subtracted southwest image. The difference image is nearly free of star-subtraction residuals for $r \sim 90'' - 180''$; the mean value of regions selected from this area, avoiding obvious residual artifacts, is used as the background value for the core image. The V -band background measurement is more straightforward and is based on a single CCD image. The regions used to measure the mean non-cluster background flux in the southwest B and V images are selected to be away from all resolved stars ($B < 16$, $V < 19$) as these are likely to be cluster members according to the Ratnatunga & Bahcall (1985) Galactic star count model (see discussion at the end of this section). The B and V background estimates show no trend with angular separation from the nearest bright star or from the cluster center, indicating that the measurements are unaffected by scattered light from bright stars or unresolved faint stars in M30.

The *HST*/WFPC2 PC1 and WF2–WF4 images are combined into a mosaic image in each of the F439W and F555W bands (GWYSB). These mosaic images are rotated, rebinned, and gaussian smoothed to match the orientation and resolution of the corresponding ground-based images (B : $0''.6 \text{ pixel}^{-1}$, FWHM $\sim 1''.5$; V : $0''.44 \text{ pixel}^{-1}$, FWHM $\sim 1''.7$). The background-subtracted ground-based images are then masked to preserve only the region of overlap with the WFPC2 mosaic, taking care to mask out the edges of both images where the smoothing of the latter is imperfect. The ground-based V image covers all of the WFPC2 F555W image, while the B image covers about 93% of the WFPC2 F439W image, excluding only a small corner section of WF2 at $r \gtrsim 1'$ from the cluster center. The resulting *HST* images differ from the corresponding ground-based images only in terms of a photometric scale factor and the background flux in the WFPC2 images.

The WFPC2 background flux in each band is obtained in two different ways. The first method involves a linear least squares fit to solve simultaneously for the photometric scale factor and WFPC2 background flux level by doing a pixel-to-pixel comparison of the $10^4 - 10^5$ pixels in each pair of matched WFPC2 and ground-based images. Because of its high stellar surface density, coupled with inaccuracies in the PSF match, the PC1 CCD is not used in this comparison. The WFPC2 background flux is estimated to be 0.0083 ADU in F439W and 0.092 ADU in F555W per $0''.0996 \times 0''.0996$ mosaic image pixel. Unless otherwise mentioned, these least-squares-fit–based WFPC2 background values are adopted

for the rest of the paper. In the second, more direct, method of background determination, the photometric scale factor is estimated using aperture photometry on a selection of bright stars which are known to be isolated on the original, high-resolution *HST* images. After applying this multiplicative photometric correction to the ground-based image, a difference image (WFPC2 minus ground-based) is constructed whose mean value should be equal to the WFPC2 background flux. In practice, point spread function (PSF) matching and star subtraction are not perfect, so it is necessary to estimate the mean background level in regions away from bright star residuals. A comparison of the two background estimates and errors in the background flux determination are discussed in § 2.2 and § 2.3.

The adopted WFPC2 background levels correspond to sky brightnesses of $\mu_{\text{sky}}(B) = 24.84 \text{ mag arcsec}^{-2}$ and $\mu_{\text{sky}}(V) = 21.45 \text{ mag arcsec}^{-2}$, but it should be noted that these background brightness levels may be partly instrumental in origin—the Space Telescope Science Institute pipeline bias subtraction may have been inaccurate seeing as the data were obtained only a few months after the installation of the WFPC2 instrument. Spatial variations in sky brightness due to individual Galactic field stars are expected to be unimportant. For example, the Ratnatunga & Bahcall (1985) Galactic star count model prediction in this part of the sky is less than 1 star arcmin⁻² with $V < 20$ at the bright end of the stellar distribution, which corresponds to a brightness level of $\mu(V) \sim 29 \text{ mag arcsec}^{-2}$. Since Galactic stars tend to outnumber distant field galaxies for $V \lesssim 21$ (cf. Bahcall, Guhathakurta, & Schneider 1990), the effect of stochastic variations in the bright end of the field galaxy population is likely to be even smaller.

2.2. Color Profile of the Cluster Starlight

This study adopts the eight radial bins defined in GWYSB for the purpose of studying M30’s $B - V$ color profile. The radial bins are chosen such that each contains approximately the same number of evolved stars with $V \lesssim 19$, a sample dominated in number by faint RGB stars. These bins are: (1) $r < 5''.00$, (2) $5''.00 \leq r < 9''.80$, (3) $9''.80 \leq r < 15''.41$, (4) $15''.41 \leq r < 23''.2$, (5) $23''.2 \leq r < 35''.8$, (6) $35''.8 \leq r < 51''$, (7) $51'' \leq r < 71''$, and (8) $71'' \leq r < 130''$. The characteristic radius adopted for each of these bins, for the purpose of comparison with model predictions, is the median radial distance of the stars in that bin (Table 2). As described in GWYSB, the total B and V flux within each radial bin is derived from direct aperture photometry on the background-subtracted WFPC2 F439W and F555W mosaic images, respectively, by differencing successive concentric circular apertures. The contribution of specific stellar populations, on the other hand, is determined by summing over the list of detected stars for which photometry has been carried out using

standard techniques (PSF fitting, aperture photometry). Only bright RGB and horizontal branch (HB) stars are analyzed in this manner for the purpose of uniform redistribution (§ 2.3). Detailed image simulations indicate that the detection rate for these bright stars is practically 100% (Yanny et al. 1994; Guhathakurta et al. 1996) so that it is not necessary to apply any radially-dependent incompleteness correction.

The mean $B - V$ color of M30 within each radial bin (annulus) is plotted in the top panel of Figure 1 (long dashed line with bold triangles). Monte Carlo realizations, based on a synthetic V -band luminosity function and $B - V$ color distribution to mimic the properties of M30’s stellar distribution, show that Poisson fluctuations in the bright RGB and HB population result in a random error of $\delta(B - V) = 0.084$ mag for each radial bin. There is a significant radial gradient of about $+0.3$ mag from the cluster center out to $r \sim 1'$, followed by an abrupt change of about -0.2 mag from $r = 1'$ to $r = 1'.5$. Specifically, a least squares fit of a straight line to the $B - V$ vs $\log(r)$ profile results in a best-fit slope of 0.13 ± 0.06 using all eight radial bins, and 0.20 ± 0.07 using only radial bins 1–7 ($r \lesssim 1'$). These measurements are in keeping with earlier observations of M30’s central blueing trend (cf. Cordoni & Aurière 1984; Peterson 1986; Piotto et al. 1988; Burgarella & Buat 1996). Note, the revised WFPC2 background flux estimates (§ 2.1) result in a color profile that is somewhat different from that published by GWYSB using the same data set, especially for $r \gtrsim 40''$. The open circles and horizontal bars show the ground-based color measurements presented by Peterson (1986). Peterson’s measurements in concentric circular apertures are converted to colors in annuli by differencing successive apertures; note, these measurements are drawn from complete annuli, while the WFPC2 image geometry forces radial bins to have incomplete azimuthal coverage beyond $r \gtrsim 15''$. Nevertheless, our *HST*-based and Peterson’s ground-based measurements of the color profile are in good agreement. The slight overall difference in $B - V$ color (≈ 0.05 mag in the mean) between the two data sets could be the result of systematic differences in photometric calibration.

The effect of the errors in background flux measurements on the final color profile is calculated in two ways:

- The formal error estimate is derived from the least squares fit to the matched WFPC2 and ground-based pixels in the WF CCDs only: the error in the mean background flux over this area is transformed to the error per WFPC2 mosaic pixel by multiplying by $\sqrt{N_{\text{WFPC2}}(3\text{WF})}$, where $N_{\text{WFPC2}}(3\text{WF}) \approx 3 \times 800 \times 800$ is the number of mosaic pixels in the area of the fit (3WF). In the photometric scale of the WFPC2 data set, the formal errors are 3.1 ADU in F439W and 2.0 ADU in F555W per mosaic pixel. The effect of WFPC2 background error on each radial bin is then computed by scaling the pixel-to-pixel error by the square root of the number of mosaic pixels in

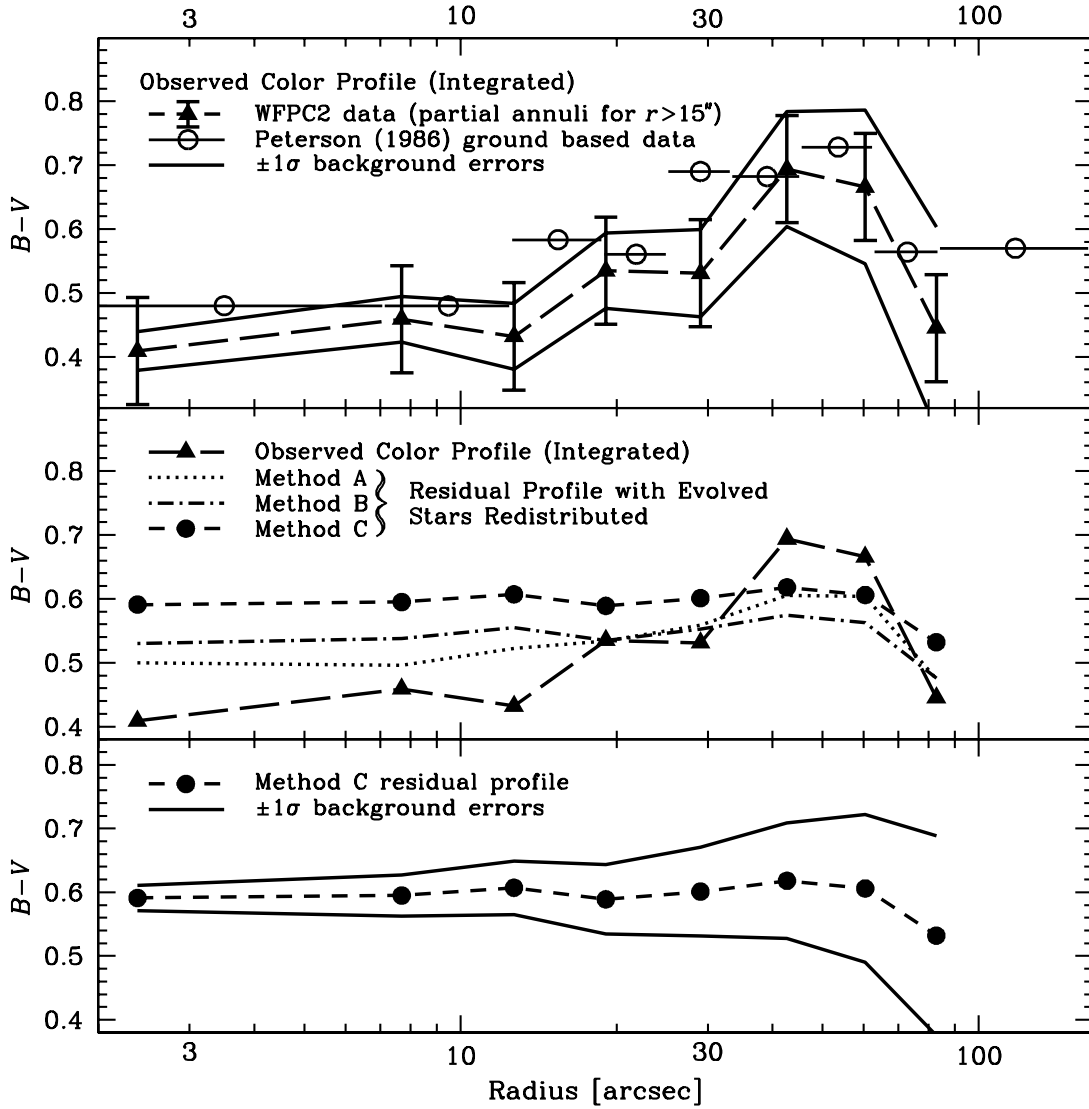


Fig. 1.— *Top panel:* The average $B - V$ color of M30’s starlight, integrated over radial bins (annuli), as a function of radius using a combination of *HST*/WFPC2 and ground-based images (long dashed line with filled triangles). The error bars account for Poisson variations in the number of bright stars in each radial bin. The solid lines illustrate the effect of $\pm 1\sigma$ conservative error estimates in the background flux level as described in § 2.2. Open circles with horizontal bars show the ground-based color measurements made by Peterson (1986). *Middle panel:* Residual $B - V$ color profiles after uniform redistribution of the light of bright red giant branch and horizontal branch stars using three different algorithms— Method A: proportional to overall cluster $B + V$ light as in GWYSB (dotted line); Method B: proportional to faint RGB stars using overall bright to faint RGB ratio (dot-dashed line); and Method C: proportional to faint RGB stars using bright to faint RGB ratio in radial bins 5–8 (short dashed line with filled circles). Method C is the most accurate redistribution algorithm; see § 2.3 for a complete discussion of the various redistribution schemes. The long dashed line and filled triangles represent the color profile of the cluster prior to redistribution (same as upper panel). The original color profile is jagged, becoming redder by about +0.3 mag from the center out to $r \gtrsim 1'$, while redistribution of HB and bright RGB flux results in a smooth profile that is consistent with no residual color gradient. *Bottom panel:* The Method C redistributed color profile (short dashed line with bold circles, as in the middle panel), with the effect of $\pm 1\sigma$ conservative background errors on the redistributed color profile illustrated by the solid lines.

that radial bin.

- The conservative error estimate is obtained by performing an independent least squares analysis on each of the three WF CCDs. The variation in the mean background flux amongst the three WF CCDs is substantially larger than the formal error in the mean given by the fitting routine. This variation is likely a result of systematic errors arising from PSF mismatch and/or bias subtraction differences from CCD to CCD. Radial bin 7 has an area comparable to that of a single WF CCD, so a conservative error for bin 7 is derived from the spread of mean background values amongst the three WF CCDs: the spread in the mean is scaled by the number of pixels in each fit (the number of matched pixels in each WF CCD) to convert the error in the mean to an error in the sum, and multiplied by the square root of the ratio of the area of bin 7 to that of a WF CCD, $\sqrt{A(\text{radial bin 7})/A(\text{WF})}$. The background errors for the other radial bins ($i = 1, 8$) are estimated in similar fashion by multiplying by $\sqrt{A(\text{radial bin } i)/A(\text{WF})}$. The conservative error estimate for radial bin 7 is (practically) free of the assumption that the error in the background flux scales as the square root of the area since $\sqrt{A(\text{radial bin 7})/A(\text{WF})} = 0.93$. This area ratio factor departs most strongly from unity for the innermost bins, but then the background flux (and the error in the background) is a negligible fraction of the total flux in these bins.

The error in the measurement of the background level in the ground-based images is determined from the variance amongst mean values in different blank regions. The variance is scaled to the area of each radial bin and is added in quadrature to the WFPC2 background error (formal and conservative) for that bin. Note, the uncertainty in the background level of the ground-based images is generally unimportant in relation to the uncertainty in the WFPC2 background; the ground-based background error is only 20% of the overall error in the case of the formal B band error and even less in the other cases. The net B - and V - band background errors are combined in order to assess the effect on the color profile of M30's starlight; the $\pm 1\sigma$ conservative error in the background is shown by the solid lines in the top panel of Figure 1.

The formal error is about an order of magnitude smaller than the conservative error; these estimates probably represent lower and upper bounds, respectively, on the true error. In assuming \sqrt{A} scaling of the summed background flux, the formal error estimate ignores systematic errors such as PSF mismatch and possible CCD-to-CCD differences in residual bias level. The conservative error estimate, on the other hand, is derived from a comparison of the three WF CCDs which are known *a priori* to have different stellar densities and hence different degrees of systematic error caused by PSF mismatch of bright

stars. The direct measurement of the background in bright-star-free regions agrees with the background value derived from the least squares fit to the full area of the three WF CCDs to well within the conservative error (§ 2.1).

2.3. Uniform Redistribution of the Light of Evolved Stars

M30’s nucleus has been shown to be deficient in the most luminous RGB stars. The ratio of the surface density of bright RGB stars to the cluster surface brightness (Piotto et al. 1988) or to the surface density of faint RGB/subgiant stars (GWYSB) is significantly lower in the central $r < 30''$ than further out in the cluster. The central four radial bins ($r < 23''$) contain only 23 bright RGB stars, less than 40% of the expected number (60). The expected bright RGB number is derived from the observed number in radial bins 5–8 ($23'' < r < 130''$) which are unaffected by the central deficiency of these stars, normalizing to the faint RGB population; a comparable bright RGB fraction is estimated from Peterson’s (1986) ground-based data in the $r = 1'–3'$ region of the cluster. Similarly, the net bright RGB flux in the inner four radial bins is 40.9% of the flux in radial bins 5–8. Is the central deficiency of bright RGB stars entirely responsible for M30’s bluer-inward color gradient? The light from bright RGB stars must be redistributed in some *uniform* way in order to determine how much of the observed color gradient is due to this central bright RGB depletion.

In GWYSB, bright RGB flux was redistributed following the radial dependence of the total $B + V$ flux, with the relative normalization between the two bands chosen such that faint RGB stars (with the same color as the average cluster color) contribute equally in B and V . The result is the dotted curve in the middle panel of Figure 1; we refer to this as Method A. While this traditional method of bright RGB redistribution algorithm is convenient to implement, it is obviously inaccurate. In the limiting case where the population being redistributed has a negligible contribution to the overall cluster light, Method A produces uniform redistribution. In general, however, the stellar population of interest accounts for a finite fraction of the total light, so that the redistributed color profile contains a “ghost” of the original color profile. This is due to the fact that the normalizing function for redistribution—the integrated cluster light profile—is itself influenced to some degree by the original radial distribution of the stars being redistributed. Specifically, redistributing the bright RGB stars in M30 by Method A results in a larger residual bluer-inward color gradient than the more accurate methods defined below (Fig. 1), because bright RGB stars contribute 30%–50% of the total cluster light.

A more reasonable scheme might be to redistribute the bright RGB light in proportion

to the faint RGB stars. For example, this may be achieved by assigning one eighth of the total bright RGB flux to each radial bin (dot-dashed curve in middle panel of Fig. 1; Method B), since the radial bins were defined to contain approximately equal numbers of faint RGB stars. Note, however, that the total bright RGB flux in the WFPC2 image of M30 is lower than it would have been in the absence of the central bright RGB depletion. Making the assumption that the relative abundance of the bright RGB population is ‘normal’ beyond $r \sim 25''$ in M30, the preferred method of redistribution is to assign one fourth of the bright RGB flux summed over radial bins 5–8 to each of the 8 radial bins, again roughly in constant proportion to faint RGB stars (Method C; short dashed line and solid circles in middle and bottom panels of Fig. 1). Unlike the other redistribution methods, Method C actually adds in extra bright RGB flux to compensate for the central bright RGB deficiency in the cluster. If there is no residual color gradient, this simply has the effect of producing a redward color offset with respect to the Method B profile. However, if a residual color gradient is present, Method C produces both a shallower color gradient and redder overall colors than Method B because of dilution by the extra bright RGB light. The two new bright RGB redistribution methods used in this paper, Methods B and C, are coupled with redistribution of the flux of HB stars: each radial bin is assigned one eighth of the total HB flux, thereby correcting for Poisson noise in the distribution of HB stars and forcing the HB to faint RGB flux ratio to be constant. Table 1 summarizes the redistribution methods described above and lists both the formal and conservative error estimates. The solid lines in the bottom panel of Figure 1 show the effect of $\pm 1\sigma$ conservative background errors on the Method C residual profile.

The motivation for these redistribution schemes is that mass segregation is *not* expected to produce radial gradients in either the bright to faint RGB ratio or the HB to faint RGB ratio, as the characteristic masses of faint and bright RGB stars differ by only $\Delta M \lesssim 0.03 M_{\odot}$ (Bergbusch & Vandenberg 1992), and the typical masses of HB stars are thought to be within $0.1 M_{\odot}$ that of faint RGB stars (Lee, Demarque, & Zinn 1990). Moreover, the dynamical timescale for mass segregation is about a factor of 4 longer than the lifetime in the HB evolutionary phase (Djorgovski 1993; Lee & Demarque 1990).

Redistribution of both bright RGB and HB flux results in a residual color profile that is consistent with no residual color gradient, and quite smooth compared to the observed color profile (Fig. 1). The jagged nature of the original color gradient results from relatively small numbers of bright RGB and HB stars dominating the light at any given radius. The smoothness of the residual, redistributed color profile indicates that the photometry and subtraction of these bright evolved stars must be accurate. The slight kink in radial bin 3

TABLE 1. Methods of Redistribution for Evolved Stars

	Bright RGB	HB
Method A	Redistributed in proportion to integrated $B + V$ cluster light	Not redistributed
Method B	Redistributed in proportion to faint RGB stars, with a ratio equal to the mean bright to faint RGB ratio in the full WFPC2 sample ($r < 130''$)	Redistributed in proportion to faint RGB stars, with a ratio equal to the mean HB to faint RGB ratio in the full WFPC2 sample ($r < 130''$)
Method C	Redistributed in proportion to faint RGB stars, with a ratio equal to the mean bright to faint RGB ratio in the outer four radial bins ($23'' < r < 130''$) ^a	Redistributed in proportion to faint RGB stars, with a ratio equal to the mean HB to faint RGB ratio in the full WFPC2 sample ($r < 130''$)

^aMethod C involves a net *addition* of bright RGB light to the inner regions of M30 to compensate for the central depletion of these stars; strictly speaking, it is therefore not a redistribution scheme.

may be due to oversubtraction at the level of 1–2%. A χ^2 test shows that a constant color (no gradient) is an adequate fit to the Method C residual color profile, and no significant slope is found.

The fraction of B - and V -band light from evolved stars, defined to be those with $V < 18.6$ (bright/faint RGB, HB, subgiants, blue stragglers), is measured in each radial bin after uniform redistribution of bright RGB and HB stars using Method C. These fractions, $f_{\text{ev}}(V)$ and $f_{\text{ev}}(B)$, are shown in Figure 2 (bold and open squares) and listed in Table 2. Evolved stars contribute about three quarters of the total flux at small radii in both bands and their flux fraction falls off with increasing radius to about 0.6 at $r \gtrsim 1'$. The $f_{\text{ev}}(V)$ fractions are needed for appropriate normalization of the models in §3.3; the observed $f_{\text{ev}}(V)$ and $f_{\text{ev}}(B)$ values are also compared to fractions derived from the Bergbusch & Vandenberg (1992) theoretical luminosity function (§3.4). Although f_{ev} is calculated after evolved star redistribution, these values will be referred to as “observed” f_{ev} values for the rest of this paper.

3. Effect of Main Sequence Mass Segregation

3.1. Dynamical Models

A Fokker-Planck (FP) dynamical model (Dull et al. 1997) designed specifically for the cluster M15, constrained by its measured velocity dispersion, surface brightness profile, and millisecond pulsar acceleration, is used in this paper. No FP model has been designed for M30, so the M15 model is adapted to M30 by applying a small adjustment to its radial scale (B. W. Murphy 1998, private communication). Additional procedures used to tailor the model to M30 are described in §3.3. There are important differences between the physical parameters of M15 and M30 some of which may even be relevant to the central depletion of bright red giants—e.g., M15’s central velocity dispersion and central density are about twice the corresponding M30 values (Dubath, Meylan, & Mayor 1997; Pryor & Meylan 1993). However, the FP model is merely used to characterize mass segregation in M30, recognizing that the model is not expected to apply to M30 in detail. The effect of varying the nature and degree of mass segregation is explored in §§3.3–3.4.

The FP model specifies the number of stars in each of twenty stellar mass bins as a function of radius. The first five mass bins represent nonluminous stellar remnants (neutron stars and white dwarfs of various masses) which are irrelevant for the color gradient computation. The next two mass bins correspond to HB and RGB stars, respectively, and the last thirteen mass bins cover main sequence stars of successively lower mass in the range

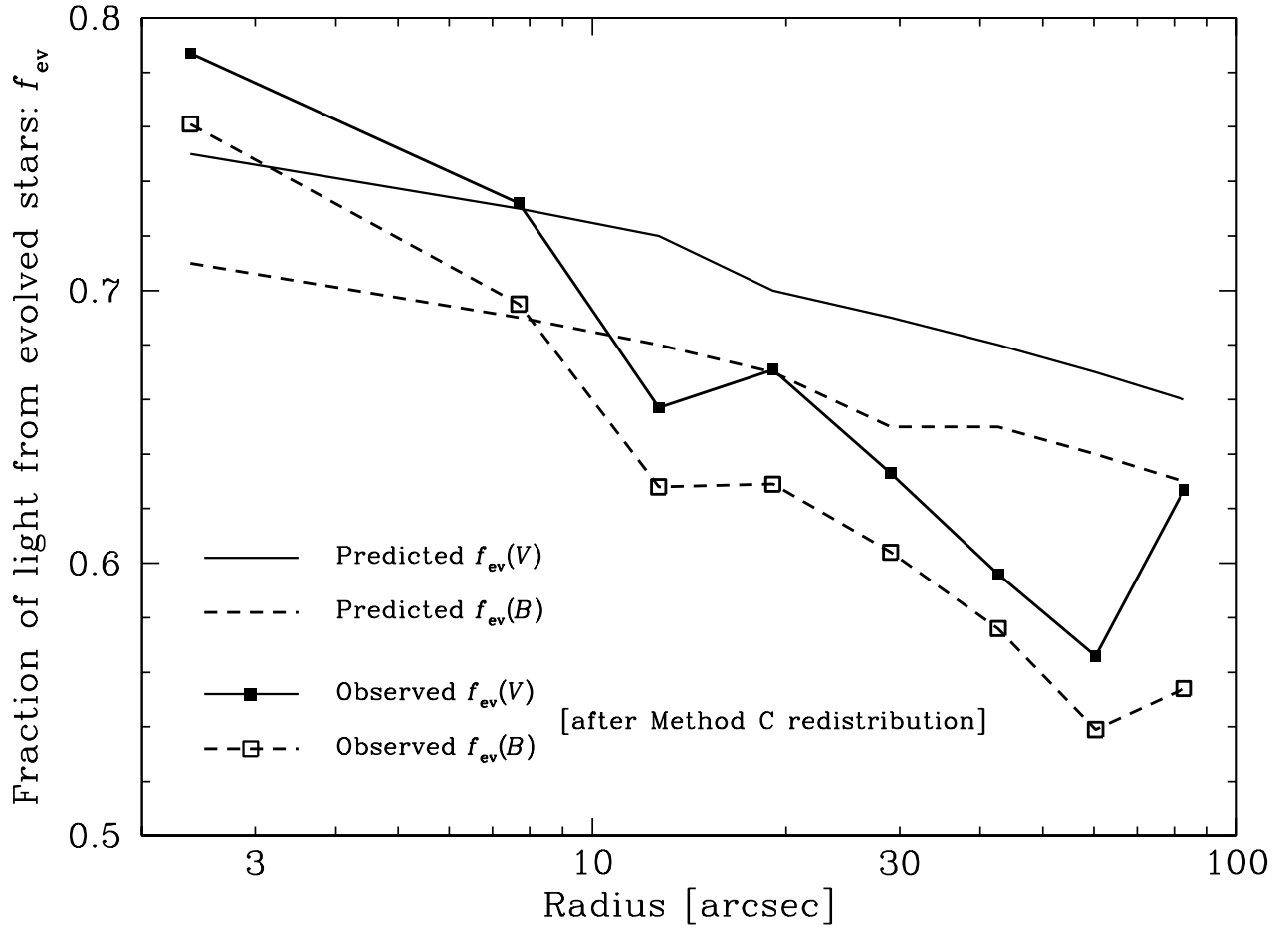


Fig. 2.— The ratio of the light of evolved stars ($V < 18.6$) to the light of all stars, f_{ev} , as a function of radius in M30. The ‘observed’ f_{ev} values in the B and V bands represent measurements made after the bright RGB and HB stars have been redistributed via Method C (dashed line with open squares and solid line with filled squares, respectively). Predictions based on the Bergbusch & Vandenberg (1992) 10 Gyr theoretical isochrones are shown as dashed and solid lines (without symbols) for the B and V bands, respectively. The redistributed evolved star fraction in both bands falls progressively below the theoretical prediction with increasing radius beyond $r \sim 10''$.

$0.74 - 0.11 M_{\odot}$. The model mass functions are not strictly monotonic with stellar mass at all radii, though they display a general increase in number of stars towards smaller stellar mass, more so at large radii than at small radii.

As an alternative to the FP dynamical model, a multimass KM is also considered. Although PCC clusters are thought to be in a nonequilibrium state, multimass KMs provide an adequate description of the observed variation in mass function slope as a function of radius (cf. Sosin & King 1997). Bolte (1989) derived the mass function slope at $r \approx 100'' - 400''$ in M30 from studies of the luminosity function of faint main sequence stars, and fit the data with a multimass KM from Pryor, Smith, & McClure (1986) using an assumed core radius of $10''$ (see Fig. 3 of Bolte 1989). In the present study, this KM is used to predict the mass function slope x as a function of radius in the inner part of M30: $x = -2.75$ in radial bin 1 ($r \sim 2''$) and $x = +0.25$ in radial bin 8: ($r \sim 80''$). Note x is defined in the usual way: $dN(M) \propto M^{-(1+x)}dM$.

3.2. Stellar Evolution Models

Theoretical stellar isochrones provide the luminosity and color of stars as a function of their mass. We use a Bergbusch & Vandenberg (1992) isochrone with $[\text{Fe}/\text{H}] = -2.03$, $[\text{O}/\text{Fe}] = +0.70$, and $Y = 0.235$, consistent with the estimated abundance of M30 (cf. Zinn & West 1984; Carretta & Gratton 1997; Sandquist et al. 1999). The calculations presented in this paper are based on a 10 Gyr isochrone; the main result, however, is insensitive to choice of isochrone age. Bergbusch & Vandenberg compute evolutionary tracks in $(M_V, B - V)$ space as well as stellar luminosity functions for a variety of power law initial mass function slopes.

Recently, D’Antona and collaborators have calculated stellar evolutionary tracks using updated input physics (P. Ventura 1998, private communication). The models are based on the assumption of gray atmospheres for stellar masses $M > 0.6 M_{\odot}$ (Silvestri et al. 1998) and use model atmospheres from Hauschildt, Allard, & Baron (1999) and Allard et al. (2000) for $M < 0.6 M_{\odot}$ (Montalbán et al. 2000). The Castelli (1998) conversion from effective temperature to $B - V$ color is used in both mass ranges. Our study uses the 10 Gyr, $[\text{Fe}/\text{H}] = -2$ isochrone from D’Antona’s group; this is hereafter referred to as the “D’Antona” theoretical isochrone. The lower main sequence portion of the D’Antona isochrone ($M_V > 9$) is bluer by up to $\Delta(B - V) = -0.2$ mag than the Bergbusch & Vandenberg (1992) isochrone. Moreover, stars of a given mass are brighter by as much as -0.5 mag in M_V in the former isochrone. These differences have a negligible impact on the predicted overall $B - V$ color profile (§ 3.3; Table 2).

3.3. Predicted Color Gradient

The dynamical models and stellar isochrones described above are used to compute the $B - V$ color of the cluster light as a function of radius. For computational convenience and by analogy with the M30 data set, the dynamical models are normalized to a fixed number of red giants in each of the 8 radial bins. The radii in the dynamical models are compared directly to the observed (projected) radii in M30; projection effects are ignored since M30’s radial brightness profile is relatively steep. If anything, projection tends dilute the model color gradient. Whereas, as we show below, the color gradient predicted by mass segregation models is already very small.

In the case of the FP dynamical model, mass bin #7 represents red giants and contains stars with mass $M \sim 0.8 M_{\odot}$ covering a wide range of absolute magnitudes: $M_V \approx -2.7$ (tip of RGB) to $M_V \approx +3.6$ (main sequence turnoff). What is the appropriate stellar luminosity to attach to this mass bin? A direct flux-weighted integration of M30’s observed evolved star luminosity function in the V and B bands over the range $M_V < +3.6$ yields a characteristic absolute magnitude of $(M_V)_{\text{RGB}} = +1.2$ and a color of $(B - V)_{\text{RGB}} = +0.80$ for the set of red giants, subgiants and turnoff stars represented by mass bin #7. The HB stars in the FP dynamical model (mass bin #6) are tailored specifically to M15, and M30 has a significantly different HB morphology and HB to RGB ratio. Each HB star is assigned an absolute magnitude of $(M_V)_{\text{HB}} = +0.45$ and a color of $(B - V)_{\text{HB}} = -0.05$, as measured for M30’s short blue HB. The total number of HB stars predicted by the FP model across all 8 radial bins is scaled so that the overall HB/RGB V -band flux ratio matches that observed in M30 (after correcting for central bright RGB depletion), while preserving the FP model’s run of HB/RGB ratio with radius (monotonic increase outward). Main sequence stars in mass bins #8–#20 are assigned B and V luminosities based on the Bergbusch & Vandenberg (1992) evolutionary tracks.

As a further adaptation of the FP model to M30, the number of evolved stars (RGB+HB, mass bins #6 and #7) is adjusted with respect to the number of main sequence stars (sum of mass bins #8–#20). The adjustment is carried out independently in each radial bin to ensure that the fractional evolved star V -band flux, $f_{\text{ev}}(V)$, in the model agrees with the ‘observed’ value in that radial bin of M30, after uniform redistribution of RGB and HB stars (§ 2.3; Table 2). This method of normalizing to the observed $f_{\text{ev}}(V)$ values is preferred over a direct integration of the model because M30 is observed to have a 30% higher RGB-to-turnoff ratio than predicted by models (Sandquist et al. 1999; GWYSB). At each radius, the overall luminosities in the B and V bands are obtained by integrating over stars in all the model mass bins. This yields the predicted $B - V$ color of M30 as a function of radius (“FP” entry in Table 2).

TABLE 2. Color Gradient and Fractional Evolved Star Flux Model Predictions

Radial Bin # Char. Radius	(1) 2''38	(2) 7''70	(3) 12''68	(4) 19''07	(5) 29''04	(6) 42''66	(7) 60''40	(8) 82''82
$(B - V)_{M30, \text{obs}}^{\text{a}}$	0.409	0.459	0.432	0.535	0.531	0.694	0.666	0.445
Formal σ_{B-V}	0.002	0.003	0.004	0.004	0.005	0.006	0.009	0.013
Conservative σ_{B-V}	0.030	0.036	0.052	0.059	0.068	0.090	0.12	0.16
$(B - V)_{M30, \text{residual}}^{\text{b}}$	0.591	0.595	0.607	0.589	0.601	0.618	0.606	0.532
Formal σ_{B-V}	0.001	0.002	0.003	0.004	0.005	0.007	0.009	0.012
Conservative σ_{B-V}	0.020	0.032	0.042	0.055	0.069	0.091	0.12	0.16
$(B - V)_{\text{FP}}^{\text{c}}$	0.646	0.622	0.610	0.606	0.600	0.599	0.600	0.600
$(B - V)_{\text{KM-BV1}}^{\text{d}}$	0.644	0.630	0.604	0.600	0.595	0.591	0.591	0.592
$(B - V)_{\text{KM-DA1}}^{\text{e}}$	0.636	0.621	0.592	0.588	0.581	0.575	0.573	0.576
$(B - V)_{\text{KM-BV2}}^{\text{f}}$	0.598	0.598	0.594	0.598	0.602	0.604	0.608	0.615
$(B - V)_{\text{KM-DA2}}^{\text{g}}$	0.591	0.589	0.583	0.586	0.588	0.588	0.590	0.598
$(B - V)_{\text{KM-BV3}}^{\text{h}}$	0.545	0.543	0.543	0.543	0.543	0.544	0.545	0.547
$f_{\text{ev}}(V)$	0.79	0.73	0.66	0.67	0.63	0.60	0.57	0.63
$f_{\text{ev}}^{\text{pred}}(V)$	0.75	0.73	0.72	0.70	0.69	0.68	0.67	0.66
$f_{\text{ev}}(B)$	0.76	0.70	0.63	0.63	0.60	0.58	0.54	0.55
$f_{\text{ev}}^{\text{pred}}(B)$	0.71	0.69	0.68	0.67	0.65	0.65	0.64	0.63

^aObserved color gradient in M30

^bM30 color gradient after uniform redistribution of bright red giants and HB stars using method C (§ 2)

^cFokker-Planck dynamical model; Bergbusch & Vandenberg isochrone; empirical scaling of HB+RGB to main sequence ratio

^dSame as FP, using multimass King dynamical model

^eSame as KM-BV1, using D'Antona isochrone

^fSame as KM-BV1, with constant HB to RGB ratio

^gSame as KM-DA1, with constant HB to RGB ratio

^hSame as KM-BV2, with no scaling of RGB+HB to main sequence ratio

The above technique is repeated for the multimass KM, using power law stellar mass functions whose slope x increases with radius (§ 3.1). The calculation is performed using both sets of evolutionary tracks to attach a V -band luminosity and $B - V$ color to stars of a given mass and the results are listed in Table 2: “KM–BV1” (Bergbusch & Vandenberg 1992) and “KM–DA1” (D’Antona). As described above, the $f_{\text{ev}}(V)$ normalization constraint (ratio of evolved stars to main sequence stars) is applied at each radius; HB stars are normalized to the RGB population overall, and the radial dependence of the HB to RGB ratio is adopted from the FP model.

To be consistent with the redistribution of HB stars in M30 and following the reasoning given in § 2.3, calculations are also carried out in which the ratio of model HB to RGB flux is forced to be constant with radius and equal to the ratio measured in M30 (after bright RGB and HB redistribution). The calculations are otherwise identical to the “KM–BV1” and “KM–DA1” calculations described above. The constant HB-to-RGB results are labeled “KM–BV2” and “KM–DA2” in Table 2.

The effect of relaxing the $f_{\text{ev}}(V)$ normalization constraint is also explored. This is done via direct integration of the luminosity functions tabulated by Bergbusch & Vandenberg (1992) for mass function slopes in the range $x = 0$ to $+2.5$. The mass functions must be extrapolated to obtain the negative slopes, $x \gtrsim -3$, appropriate for M30’s central regions (§ 3.1). The Bergbusch & Vandenberg model isochrones do not include the HB phase of stellar evolution. As in the “KM–BV2” calculation, HB flux is added in constant proportion to RGB stars at all radii. The resulting $B - V$ color gradient is labeled “KM–BV3” in Table 2. Note, the $f_{\text{ev}}^{\text{pred}}(V)$ values for the Bergbusch & Vandenberg isochrone, with HB stars added in, tend to be higher than the observed values in M30 for $r \gtrsim 10''$ (with bright RGB and HB stars redistributed): the discrepancy is about 10% at $r \sim 30''$ (Table 2; Fig. 2).

Comparing the results of the six calculations described above (Table 2), it is clear that choice of dynamical model has little effect on the color profile: “FP” and “KM–BV1” model colors differ by less than ± 0.01 mag at all radii. The bluer lower main sequence in the D’Antona isochrone relative to the Bergbusch & Vandenberg (1992) isochrone (§ 3.2) results in slightly bluer overall colors, though the color gradient is nearly the same (“KM–BV1” vs “KM–DA1” and “KM–BV2” vs “KM–DA2”). Lower main sequence stars produce a larger fraction of the total light at large radii than at small radii, and this results in a slightly greater difference in color between D’Antona and Bergbusch & Vandenberg calculations at large radii. Comparing the “KM–BV1” results to “KM–BV2” and “KM–DA1” to “KM–DA2” shows that the increase in HB/RGB ratio with increasing radius in the former

set of calculations is responsible for the overall bluer colors at large radii; the constant HB/RGB ratio in the latter set of calculations yields a marginally redder-outward gradient. Unlike the other calculations, the “KM–BV3” case avoids empirical normalization of the evolved-to-main sequence flux ratio. Thus, “KM–BV3” has a higher evolved star fraction than the other cases since the Bergbusch & Vandenberg $f_{ev}^{pred}(V)$ values are generally higher than the observed $f_{ev}(V)$ values; this results in slightly bluer overall colors due to the increased prominence of evolved stars, most notably bright blue HB stars.

A back-of-the-envelope calculation based on the “KM–BV3” model illustrates why main sequence mass segregation can make no appreciable contribution to M30’s overall color gradient. The mean cluster color of about $\langle B - V \rangle_{M30} = +0.7$, which also happens to be the mean color of faint RGB stars, is a reasonable value at which to separate the main sequence into an upper and lower main sequence (UMS and LMS, respectively). Integrating the LMS, UMS, and evolved star portions of the isochrone shows that the relative numbers of stars are: $N_{LMS} \approx N_{UMS} \approx 8 N_{ev}$ in radial bin 2; and $N_{LMS} \approx 4 N_{UMS} \approx 50 N_{ev}$ in radial bin 7. Evolved stars contribute about 70% of the total light in radial bin 2, and 55% in radial bin 7. The typical evolved star (RGB/HB) is $\approx 100\times$ more luminous in V and ≈ 0.3 mag redder in $B - V$ than typical UMS stars, and $\approx 1000\times$ more luminous and ≈ 0.3 mag bluer than LMS stars. Thus, the color shift relative to the faint RGB due to UMS stars is the product of their fractional flux contribution ($0.7 \times 0.01 \times 8$) and the color difference (-0.3 mag): $\Delta(B - V) = -0.017$ mag in radial bin 2, and $\Delta(B - V) = 0.55 \times 0.01 \times (50/4) \times (-0.3) = -0.021$ mag in radial bin 7. Similar calculations for the LMS yield shifts in $\Delta(B - V)$ of $+0.002$ mag and $+0.008$ mag, respectively. The estimated net color gradient due to main sequence mass segregation from this admittedly oversimplified calculation is $\Delta(B - V) = -0.021 + 0.008 - (-0.017 + 0.002) = +0.002$ mag redder outward, well within the range of $+0.01$ mag to -0.05 mag yielded by more precise calculations, and equal to the value of $+0.002$ mag from the most closely related such calculation, “KM–BV3” (Table 2).

3.4. Fraction of Evolved Star Light

The calculation involving direct integration of the Bergbusch & Vandenberg (1992) stellar mass and luminosity functions, “KM–BV3”, predicts a larger fraction of evolved star light for $r \gtrsim 10''$ than the f_{ev} values observed in M30 (§ 2.3). Put another way, a higher fraction of main sequence light is observed than predicted, especially as one moves away from the cluster center. This discrepancy is similar in B and V . To resolve the discrepancy in the context of power law mass functions (as the multimass KMs are parameterized

above), the exponent must vary with radius from $x = -5$ in the innermost radial bin ($r \sim 2''$) to $x = 0$ around $r \sim 20''$ to $x = +1.5$ in the outermost radial bin ($r \gtrsim 1'$). However, the stellar mass function is not necessarily a power law and there may be alternate ways of resolving the f_{ev} discrepancy. Also, the true discrepancy is nearly 30% greater than Figure 2 indicates: the “KM–BV3” calculation does not take into account M30’s 30% higher ratio of RGB to turnoff stars relative to model isochrones (Sandquist et al. 1999; GWYSB).

As described in §3.1, the mass function slopes used for the KM calculations in this paper are derived from mass function measurements at $r \gtrsim 2'$ in M30 (Bolte 1989). This model-based inward extrapolation is sensitive to the choice of cluster core radius. Recent high resolution studies of the central region have shown that the effective cluster core radius is significantly smaller than Bolte’s assumed value of $r_{\text{core}} = 10''$ (Yanny et al. 1994). This would imply a somewhat stronger radial dependence of the mass function slope x over the $r \lesssim 2'$ region than we have adopted. The KM–BV3 calculations are repeated using values of $x = -5$ in the first radial bin to $x = 0$ in the outermost radial bin, where this range of x values is obtained by a simple linear extrapolation of Bolte’s data points. As the models of Pryor et al. (1986) flatten out at $x \gtrsim -3$ at small radii, this linear extrapolation is an unrealistically extreme case. The resulting color gradient is $\Delta(B - V) = -0.007$ mag bluer outward, and, like the other calculations, is consistent with the M30’s residual color profile. The more extreme mass segregation invoked to explain the discrepancy between predicted and observed f_{ev} values ($x = -5$ to $+1.5$; see previous paragraph) likewise has little net effect on the color gradient.

The fractional degree of contamination by faint red foreground field stars is expected to increase radially outward—e.g., the area of radial bin 1 is 79 arcsec^2 while that of radial bin 8 is 8440 arcsec^2 , even though both bins contain roughly the same number of cluster giants. However, the density of M30 stars is so high in the central region of the cluster covered by the WFPC2 image that field star contamination should be negligible even in radial bin 8. The number of field stars predicted by the Galactic star count model of Ratnatunga & Bahcall (1985) is too low by several orders of magnitude to have a significant effect on M30’s color profile.

4. Conclusions

The radial $B - V$ color profile of the post core collapse cluster M30 is measured using *Hubble Space Telescope* Wide Field Planetary Camera 2 images, along with ground-based images whose wider field of view allows for a reliable determination of the non-cluster background in the WFPC2 image. M30 displays a significant

radial color gradient of $\Delta(B - V) \sim +0.3$ mag, corresponding to a slope of $\Delta(B - V)/\Delta \log(r) = 0.20 \pm 0.07$ mag dex⁻¹ from $r = 2'' - 1'$. An accurate new technique is developed for uniform redistribution of the light of the brightest cluster stars, which compensates for stochasticity in their spatial distribution and for the central depletion of bright red giants. There is no significant residual color gradient after bright star redistribution, implying that post-main-sequence stars are entirely responsible for the central color gradient in M30. This is contrary to the recent results of GWYSB and Burgarella & Buat (1996), but confirms the earlier finding of Piotto et al. (1988).

The physical mechanism responsible for the central depletion of bright red giants (and hence the color gradient) in M30 and in other post-core-collapse clusters remains a mystery. Direct stellar collisions are too infrequent to destroy an appreciable fraction of the giants within their short lifetimes. The lack of a comparable central depletion amongst horizontal branch stars, the downstream evolutionary products of bright red giants, suggests a ‘short circuiting’ of the bright red giant phase rather than complete destruction of such stars; this may bear some relation to the evolution of giants in binary systems. The reader is referred to Djorgovski et al. 1991 and GWYSB and to references therein for a detailed discussion of these issues.

This study also investigates the effect on the color profile of mass segregation of main sequence stars in the context of cluster dynamical models and theoretical stellar isochrones. The model calculations show a slight bluer-outward color gradient when the HB varies as predicted by the Fokker-Planck dynamical model [$\Delta(B - V) \sim -0.06$ from $r = 20'' - 80''$], and an even smaller redder-outward gradient if the HB is held constant with respect to the RGB. In all cases, the color gradient predicted by mass segregation models is consistent with the data to within the measurement uncertainties. The predicted fraction of light from evolved stars using the theoretical mass and luminosity functions of Bergbusch & Vandenberg (1992) suggests that there is a 10%–30% achromatic excess of faint star light at large radii in M30 relative to conventional mass segregation models.

We would like to thank Brian Murphy for providing an updated electronic version of the Fokker-Planck models described in Dull et al. (1997), Paolo Ventura for providing the isochrones computed by D’Antona’s group, and Mike Bolte for providing ground-based images. We are grateful to Sandy Faber and Mike Bolte for a critical reading of the manuscript, and to the referee, George Djorgovski, for several insightful comments. PG would like to thank his collaborators on the M30 WFPC2 study, Zo Webster, Brian Yanny, Don Schneider, and John Bahcall, for useful discussions about M30’s color gradient in

the context of an earlier paper that served as the motivation for this work. This project was supported in part by an undergraduate McNair Scholarship from the University of California at Davis (AT).

REFERENCES

- Allard, F. et al. 2000, in preparation
- Bahcall, J. N., Guhathakurta, P., & Schneider, D. P. 1990, *Science*, 248, 178
- Bergbusch P., & Vandenberg, D. A. 1992, *ApJS*, 81, 163
- Bolte, M. 1987, *ApJ*, 319, 760
- Bolte, M. 1989, *ApJ*, 341, 168
- Burgarella, D., & Buat, V. 1996, *A&A*, 313, 129
- Carretta, E., & Gratton, R. G. 1997, *A&AS*, 121, 95
- Castelli, F. 1998, *M. S. A. It.*, 69, 165
- Chun, M. S., & Freeman, K. C. 1979, *ApJ*, 227, 93
- Cordoni, J.-P., & Aurière, M. 1984, *A&AS*, 58, 559
- Djorgovski, S. G. 1993, in *ASP Conf. Ser. 50, Structure and Dynamics of Globular Clusters*, ed. S. G. Djorgovski & G. Meylan (San Francisco: ASP), 373
- Djorgovski, S. G., & Piotto, G. 1992, *AJ*, 313, 129
- Djorgovski, S. G., & Piotto, G. 1993, in *ASP Conf. Ser. 50, Structure and Dynamics of Globular Clusters*, ed. S. G. Djorgovski & G. Meylan (San Francisco: ASP), 203
- Djorgovski, S. G., Piotto, G., Phinney, E. S., & Chernoff, D. F. 1991, *ApJ*, 372, L41
- Dubath, P., Meylan, G., & Mayor, M. 1997, *A&A*, 324, 505
- Dull, J. D., Cohn, H. N., Lugger, P. M., Murphy, B. W., Seitzer, P. O., Callanan, P. J., Rutten, R. G. M., & Charles, P. A. 1997, *ApJ*, 481, 267
- Guhathakurta, P., Webster, Z., Yanny, B., Schneider, D. P., & Bahcall, J. N. 1998, *AJ*, 116, 1757 (GWYSB)
- Guhathakurta, P., Yanny, B., Schneider, D. P., & Bahcall, J. N. 1996, *AJ*, 111, 267
- Hauschildt, P. H. Allard, F., & Baron, E. 1999, *ApJ*, 512, 377
- Hut, P., McMillan, S. L. W., Goodman, J. J., Mateo, M., Phinney, E. S., Pryor, C., Richer, H. B., Verbunt, F., & Weinberg, M. D. 1992, *PASP*, 104, 981

- King, I. R. 1962, *AJ*, 67, 471
- Lee, Y.-W., & Demarque, P. 1990, *ApJS*, 73, 709
- Lee, Y.-W., Demarque, P., & Zinn, R. 1990, *ApJ*, 350, 155
- Meylan, G., & Heggie, D. C. 1997, *Astron. Astrophys. Rev.*, 8, 1
- Montalban, J. et al. 2000, *ApJ*, in preparation
- Peterson, C. J. 1986, *PASP*, 98, 192
- Piotto, G., King, I. R., & Djorgovski, S. 1988, *AJ*, 96, 1918
- Pryor, C., & Meylan, G. 1993, in *ASP Conf. Ser. 50, Structure and Dynamics of Globular Clusters*, ed. S. G. Djorgovski & G. Meylan (San Francisco: ASP), 357
- Pryor, C., Smith, G. H., & McClure, R. D. 1986, *AJ*, 92, 1358
- Ratnatunga, K., & Bahcall, J. 1985, *ApJS*, 59, 63
- Sandquist, E. L., Bolte, M., Langer, G. E., Hesser, J. E. & De Oliveira, C. M. 1999, *ApJ*, 518, 262
- Silvestri, F., Ventura, P., D’Antona, F., & Mazzitelli, I. 1998, *ApJ*, 509, 192
- Sosin, C., & King, I. R. 1997, *AJ*, 113, 1328
- Williams, T., & Bahcall, J. N. 1979, *AJ*, 232, 754
- Yanny, B., Guhathakurta, P., Schneider, D. P., & Bahcall, J. N. 1994, *ApJ*, 435, L59
- Zinn, R., & West, M. J. 1984, *ApJS*, 55, 45